Overturning Circulation in an Eddy-Resolving Model: The Effect of the Pole-to-Pole Temperature Gradient

CHRISTOPHER L. WOLFE AND PAOLA CESSI

Scripps Institution of Oceanography, University of California, San Diego, La Jolla, California

(Manuscript received 24 January 2008, in final form 21 July 2008)

ABSTRACT

The effect of the pole-to-pole surface temperature difference on the deep stratification and the strength of the global meridional overturning circulation (MOC) is examined in an eddy-resolving ocean model configured in an idealized domain roughly representing the Atlantic sector. Mesoscale eddies lead to qualitative differences in the mean stratification and the MOC compared to laminar (i.e., eddy free) models. For example, the spreading of fluid across the model's representation of the Antarctic Circumpolar Current (ACC) no longer relies on the existence of a sill in the ACC. In addition, the deep- and bottom-water masses—roughly representing North Atlantic Deep Water (NADW) and Antarctic Bottom Water (ABW), respectively—are eroded by the eddies so that their zonal and meridional extents are much smaller than in the laminar case. It is found that if the north pole temperature is sufficiently warm, the formation of northern deep water is suppressed and the middepth cell is small and weak while the deep cell is large and vigorous. In contrast, if the north pole temperature is in the range of the southern channel temperatures, the middepth cell is large and strong while the deep cell has a reduced amplitude. This result is consistent with the predictions of the laminar theory of the MOC. In contrast to the laminar theory, realistically strong deep stratification is formed even if the temperature at the northern sinking site is warmer than any temperature found in the channel. Indeed, middepth stratification is actually stronger in the latter case than the former case.

1. Introduction

Most of our understanding of the dynamics of the large-scale overturning and abyssal stratification of the ocean has come from the study of laminar models, which may be explicitly eddy free (e.g., Toggweiler and Samuels 1995, 1998; Samelson 1999, 2004) or attempt to parameterize the effects of mesoscale eddies either through large eddy viscosities/diffusivities (e.g., Samelson and Vallis 1997; Vallis 2000) or through more sophisticated isopycnal mixing schemes (e.g., Kamenkovich and Sarachick 2004; Radko 2005; Griesel and Maqueda 2006; Fučkar and Vallis 2007). Yet, several recent studies in single-basin domains have shown that explicitly resolved eddies can lead to qualitative changes in the stratification and circulation (Marshall et al. 2002; Cessi and Fantini 2004; Henning and Vallis 2004, 2005; Cessi et al. 2006). It is reasonable, then, to expect that the inclusion of explicitly resolved mesoscale eddies will lead to similar qualitative changes in the ocean's large-scale overturning and deep stratification.

a. Laminar theories

In their simplest conceptions, the laminar theories divide the global overturning circulation into three branches: a surface branch, a middepth branch, and a deep branch (see, e.g., Vallis 2006, section 16). These branches are illustrated in Fig. 1. The present study is concerned with water masses colder than the main subtropical thermocline—the intermediate, deep, and bottom waters—and their associated overturning cells. The structure of these subthermocline water masses depend sensitively on the existence and form of a zonally periodic channel [representing an idealized Antarctic Circumpolar Current (ACC)] and the temperature gradient across the channel (Vallis 2000). The only case in which the laminar theories produce realistically strong deep stratification and large-scale abyssal

Corresponding author address: Christopher L. Wolfe, Scripps Institution of Oceanography, University of California, San Diego, 9500 Gilman Drive, La Jolla, CA 92093-0213.
E-mail: clwolfe@ucsd.edu

DOI: 10.1175/2008JPO3991.1

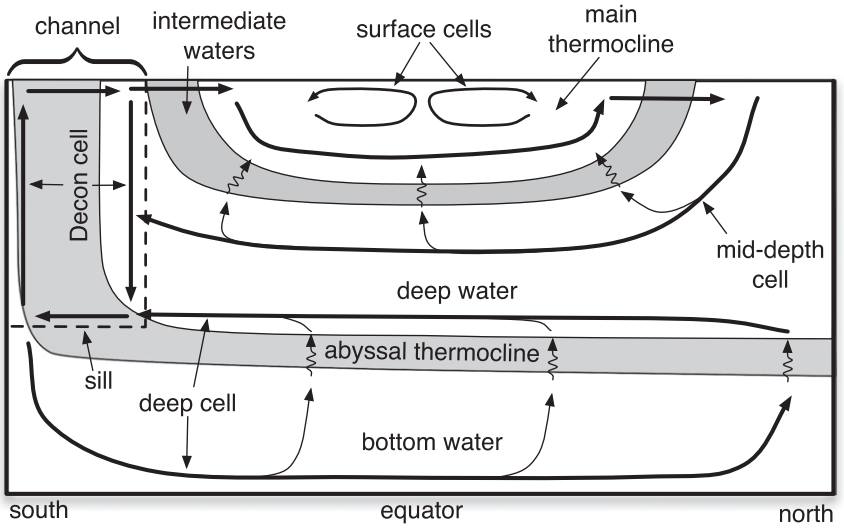

FIG. 1. Schematic of the overturning circulation in the laminar theories, consisting of three water masses—bottom water of southern origin, deep water of northern origin (separated from the bottom water by an abyssal thermocline), and thermocline water—and three overturning branches. In the case illustrated, the density of the deep water is intermediate between the densities of the channel waters (the cold pole case).

overturning is if the channel is partially blocked by a sill. Pressure gradients across the sill can then support geostrophically balanced meridional flow, allowing Southern Hemisphere ''bottom'' water to spread throughout the ocean, but only below the depth of the sill. The bottom water generally has different thermodynamic properties than the water above it, so a diffusive ''abyssal thermocline'' forms near the sill depth to adjust the properties of the water masses to each other (Stommel and Webster 1962; Young and Ierley 1986; Salmon 1990; Vallis 2000).

The importance of a source of abyssal water in the hemisphere opposite the channel depends on its density relative to the Southern Hemisphere waters. The two possible cases that are relevant to the present and near-future oceanic climate are as follows:

1) The northern water is lighter than any water found in the channel: the intermediate water formed near the equatorial edge of the channel is then denser than the northern deep water. This intermediate water then invades that Northern Hemisphere, suppressing deep-water formation. Abyssal stratification is weak and the middepth cell is absent or weak.
2) The northern water is of the same density as water found somewhere within the channel: in this case, the northern water ''splits'' and broadens the abyssal thermocline, and the layer of intermediate water above the abyssal thermocline is much shallower. The middepth cell is strongest in the Northern Hemisphere and extends to the depth of the abyssal thermocline. The diffusively driven deep cell is confined below the abyssal thermocline but extends past the latitudes of the channel. This case is illustrated in Fig. 1 and most nearly resembles the present day Atlantic Ocean.

b. *The effect of eddies*

The results of a number of recent studies (e.g., Karsten et al. 2002; Henning and Vallis 2004; Cessi and Fantini 2004; Radko and Marshall 2004; Henning and Vallis 2005; Radko 2005; Cessi et al. 2006; Hallberg and Gnanadesikan 2006; Marshall and Radko 2006) on the role of mesoscale eddies in controlling stratification and overturning require a revision of the laminar picture described above. While eddies have only a quantitative effect on the dynamics of the main thermocline in a single-hemisphere basin (Henning and Vallis 2004), the changes in the circulation and stratification in the zonal channel are profound since eddies can affect meridional transport of heat, salt, and momentum even without a mean meridional flow. Thus, unlike the laminar models, the depth of the channel stratification—and thus the depth of the global abyssal thermocline—is not constrained by the depth of the sill in the channel. Indeed, Henning and Vallis (2005), using an eddy-resolving Southern Hemisphere model, found the presence or absence of a sill had little effect on the stratification in the channel and adjacent subtropical gyre and that the abyssal thermocline was either missing or indistinguishable from the main subtropical thermocline.

These results lead to the following questions: Does the temperature of the northern sinking site relative to the channel temperature distribution still control the relative importance of the middepth and deep overturning cells? If so, what is the mechanism?

The present study seeks to make progress on this question by examining the results of a ''twin'' experiment using an eddy-resolving model configured in an idealized domain roughly representing the Atlantic Ocean plus the Atlantic sector of the Southern Ocean. In the first twin, the temperature at the northern sinking site lies within the temperature range of the channel (as in case 2 above). The second twin is identical to the first except that surface temperature is increased in the Northern Hemisphere so that the temperature at the northern sinking site is warmer than any temperature found in the channel (as in case 1 above). These two experiments will be referred to as the ''cold pole'' (CP) and ''warm pole'' (WP) cases, respectively. The model domain is a ''box'' with a flat bottom to isolate the effects of the eddies from the effects of topography and is smaller and shallower than the Atlantic Ocean to allow for long (multiple century) runs at high resolution. These experiments are similar to those of Fučkar and Vallis (2007), who studied the effect of the pole-to-pole temperature gradient in a similar domain using a coarse-resolution model with parameterized eddies.

The format of the paper is as follows: section 2 describes the configuration of the numerical model used in the twin experiment. A description of the eddy statistics and energetics, stratification, and overturning circulation of the CP configuration is given in section 3. In section 4, we describe the WP experiment with particular attention to its differences from the CP experiment. The heat flux in both experiments is discussed in section 5, and conclusions are given in section 6.

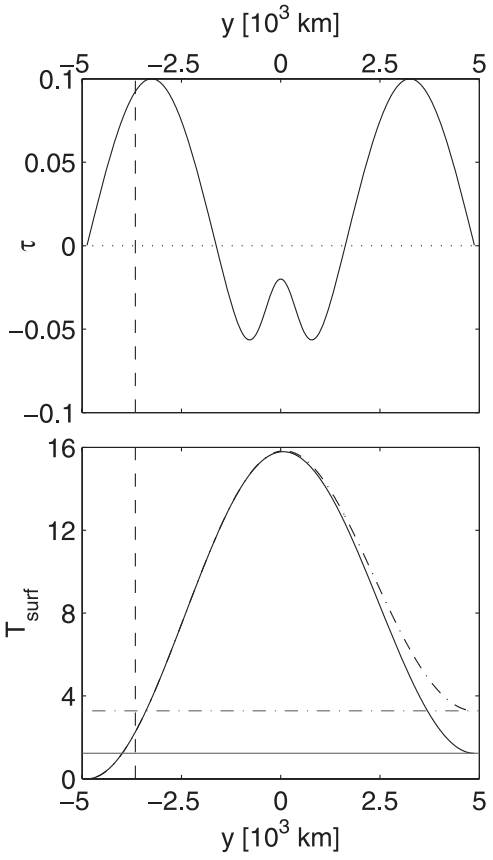

FIG. 2. Surface forcing: (top) Wind stress τ (N m^{-2}) and (bottom) surface relaxation temperature T_{surf} (°C) for the CP (solid) and WP (dashed–dotted) runs. The vertical dashed lines give the northern boundary of the reentrant channel while the horizontal gray lines give the north pole temperature of the CP (solid) and WP (dashed–dotted) runs.

2. Model configuration

We employ the Massachusetts Institute of Technology General Circulation Model (MITgcm, see Hill et al. 1999 and references therein) to integrate the hydrostatic primitive equations in a simple flat-bottomed, equatorially centered, rectangular domain with a zonally periodic channel occupying the southernmost 1200 km of the domain. In contrast to the laminar theory, in the present study the channel extends to the bottom. The approximate zonal and meridional extents of the domain are $L_x = 2400$ km and $L_y = 9800$ km, respectively, and the depth is $H = 2400$ m. This choice of domain size (narrow and shallow compared to a typical oceanic basin) was dictated by computational constraints. Experiments with a noneddy-resolving model, in which the effects of eddies are parameterized, have shown that increasing the domain size does not greatly alter the qualitative features of the circulation.

The momentum and thermodynamic equations are discretized on a fine Cartesian horizontal grid with grid spacing $\Delta x = \Delta y = 5.4$ km. The vertical grid has 20 levels with grid spacing that varies from 13 m at the surface to 274 m at the bottom. The levels are distributed such that vertical differences are second-order accurate. The use of a Cartesian grid—chosen for analytical simplicity—is somewhat nonstandard, but we have found that it does not alter the qualitative features of the circulation. Consistent with the choice of a Cartesian grid, the variation of the local planetary rotation rate is represented by a simple β plane, $f = \beta y$, with $\beta = 2.3 \times 10^{-11}$ m^{-1} s^{-1}.

The momentum equations are forced by a specified surface wind stress, shown in Fig. 2, which is an idealized and symmetrized representation of the wind stress over

the Atlantic Ocean (Hellerman and Rosenstein 1983). Dissipation is provided by horizontal Laplacian viscosity with $A_H = 12\ \mathrm{m^2\ s^{-1}}$, vertical viscosity with $A_V = 3 \times 10^{-4}\ \mathrm{m^2\ s^{-1}}$, and horizontal biharmonic friction with coefficient $A_4 = 9 \times 10^8\ \mathrm{m^4\ s^{-1}}$. The horizontal Laplacian viscosity is chosen to have the minimum value necessary to resolve the Munk layer at the western boundary and the vertical Laplacian and horizontal biharmonic friction coefficients are chosen to have the minimum value necessary to ensure numerical stability. To relieve the model of having to resolve the turbulent bottom boundary layer, the bottom boundary condition is no stress, and a linear drag with coefficient $r = 1.1 \times 10^{-3}\ \mathrm{m\ s^{-1}}$ is applied as a body force in the bottom grid cell.

Density is a linear function of temperature only, so the thermodynamic equation reduces to a forced advection–diffusion equation for the temperature. Advective fluxes are calculated using a third-order direct space–time scheme with a Sweby flux limiter, which avoids the generation of unphysical temperature extrema. Temperature is diffused via Laplacian diffusion with a constant isotropic diffusivity $\kappa = 9.8 \times 10^{-5}\ \mathrm{m^2\ s^{-1}}$, which is close to the value of $\kappa = 10^{-4}\ \mathrm{m^2\ s^{-1}}$ required by the classical advective–diffusive theories of the thermocline (Munk 1966; Munk and Wunsch 1998). The use of an isotropic diffusivity minimizes the possibility of spurious diapycnal fluxes in the presence of large isopycnal slopes (i.e., the Veronis effect, Veronis 1975) without compromising model stability. The temperature equation is forced by relaxation to a specified zonally uniform surface temperature distribution T_{surf} in the top grid point with a relaxation time scale of 11 days. The two surface temperature distributions used in this study are shown in Fig. 2. The warm pole (WP) distribution has a northern temperature that is warmer than any temperature found in the channel, while the cold pole (CP) distribution has a northern temperature that is in the range of the temperatures found in the channel.

The spatial and temporal resolution of the model are both sufficiently fine such that a convective adjustment scheme is not necessary to maintain numerical stability. Instead, static instabilities adjust naturally via hydrostatic convection, which results in the appropriate homogenization of the tracer fields as compared to nonhydrostatic convection (Marshall et al. 1998). The convection is forced to the smallest available horizontal scale (the grid scale) by the hydrostatic constraint (see, e.g., Vallis 2006, section 2.10.1), but this scale is within a factor of 2 of the horizontal scale for *non*hydrostatic convection expected from linear Rayleigh theory for the parameters used here. Thus, for the present case, hydrostatic convection is expected to give results comparable to nonhydrostatic convection at a fraction of the computational cost and avoids the spurious internal sources of energy introduced by the more traditional convective adjustment schemes.

The CP experiment was started from rest and integrated with a time step of 500 s for 118 years. The WP experiment was then initialized using output from the CP configuration, and both models were run for an additional 320 years. At this point near-statistical equilibrium had been achieved and 4-yr running averages of the dynamical variables showed little variation except for a slow ($< 0.3\ \mathrm{mK\ yr^{-1}}$) temperature drift in the bottom 250 m.

3. Cold pole experiment

We will first give an overview of the circulation in the cold pole experiment since it bears the greatest similarity to the circulation of the present Atlantic Ocean. Detailed discussion of the differences between the warm pole and CP experiments will be given in the next section. Unless otherwise noted, all quantities discussed in this section are averages over the last 13 yr of the simulation; different averaging periods do not lead to significant changes in the results.

a. Eddies

1) DISTRIBUTION

The western boundary currents (WBCs) and their zonal extensions are associated with vigorous eddy activity, as seen in Fig. 3, by the vertically averaged eddy kinetic energy density (where *eddy* is defined as a deviation from the temporal mean). These eddies are generated by instabilities of the western boundary current and thus have their greatest activity in the depths spanned by the boundary currents—approximately the upper 500 m of the water column (Fig. 4a). Eddy–eddy interactions feed energy into the barotropic mode, resulting in a strong EKE signal that penetrates to the ocean bottom. Mesoscale eddies thus represent a mechanism by which energy originating near the surface may be transferred to the abyss.

Eddy activity is also significant in the tropics, at the interface between the channel and the southern subpolar gyre, and in the eastern halves of the subpolar gyres. Most of the eddies in the northern subpolar gyre are shed from strong, narrow eastern boundary currents similar to those described by Spall (2003), Pedlosky (2003), and Pedlosky and Spall (2005), although with significant differences which will be explored in a forthcoming paper.

An additional source of eddy activity is trapped near the western boundary at about 1000-m depth and stretches from 1500 km north to 1500 km south of the equator. This is a signature of the unstable deep western

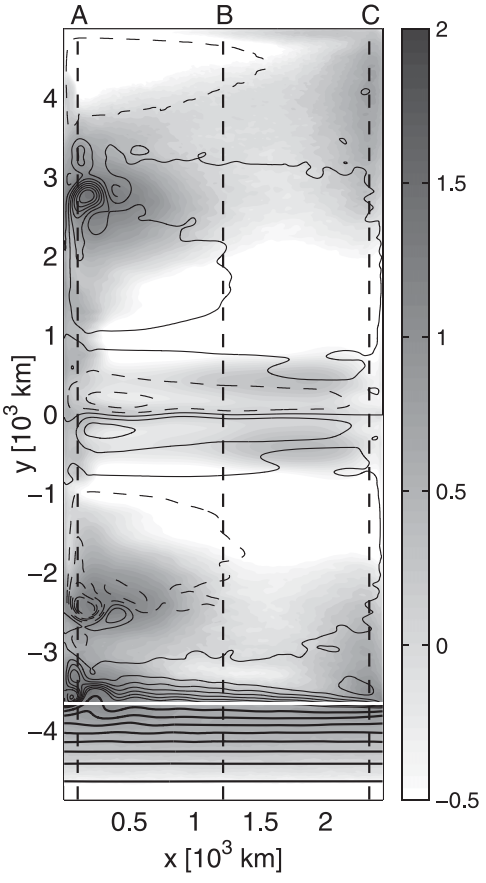

FIG. 3. Barotropic streamfunction (contours) and the $\log_{10}$ of the vertically averaged EKE (shading) in units of J kg^{-1} for the CP case. The contour interval is 5 Sv except in the channel where the contours are thick and the contour interval is 20 Sv. Negative contours are dashed. The sense of the circulation is clockwise around maxima. The northern edge of the channel is shown by the horizontal white line. Thick vertical dashed lines give the location of meridional sections shown in Fig. 4.

boundary currents (DWBC) associated with the northern and southern overturning cells.

2) ENERGETICS

Eddy kinetic energy is dissipated by bottom drag and internal viscosity. Since the eddies are not directly forced by the wind (which is stationary and has large scales), they must extract energy from the mean flow to maintain themselves against dissipation. Eddies can interact with the mean flow either through net conversion $\mathcal{C}$ of potential energy (PE) into eddy kinetic energy (EKE):

$$\mathcal{C} = \alpha\rho_0 g\overline{w'T'}, \tag{1}$$

where α is the thermal expansivity of seawater, or through direct conversion of mean KE into EKE through Reynolds stresses:

$$\mathcal{R} \equiv \mathcal{R}_H + \mathcal{R}_V = \nabla_H\bar{\mathbf{u}}_H : \mathbf{T}_H + \frac{\partial\bar{\mathbf{u}}_H}{\partial z}\cdot\mathbf{T}_V, \tag{2}$$

where

$$\mathbf{T}_H = \rho_0\begin{pmatrix}\overline{u'u'} & \overline{u'v'}\\ \overline{v'u'} & \overline{v'v'}\end{pmatrix}, \quad \mathbf{T}_V = \begin{pmatrix}\overline{w'u'}\\ \overline{w'v'}\end{pmatrix} \tag{3}$$

are a matrix of horizontal Reynolds stresses and a vector of vertical Reynolds stresses, respectively. The conversion terms $\mathcal{C}$ and $\mathcal{R}_H$ are associated with baroclinic and barotropic instability processes, respectively (Pedlosky 1987, section 7.3). The vertical Reynolds stresses $\mathcal{R}_V$ may be associated with either baroclinic instability or vertical shear instability. In the present case, $\mathcal{R}_V$ is at least an order of magnitude smaller than either $\mathcal{C}$ or $\mathcal{R}_H$ and will henceforth be neglected.

Conversion $\mathcal{C}$ of PE into EKE accounts for roughly two-thirds of the energy put into the eddy field (Fig. 5a). Here $\mathcal{C}$ is largest near the northern boundary of the channel—especially near the eastern and western boundaries where the isotherms are steepest. The unstable currents found in the eastern subpolar gyres (discussed in the previous section) are also associated with very thin, but strong, regions of baroclinic instability. Horizontal temperature gradients become small away from the boundaries and the creation of eddy energy via baroclinic instability correspondingly weaker: $\mathcal{C}$ is weakly positive in the western half of the subpolar gyres and essentially zero in the middle of the subtropical gyres.

The WBC extensions are strong regions of baroclinic instability, but the conversion of PE into EKE in the near field of the extension is compensated by conversion of EKE back into PE in the far field and near the western boundary. Thus, the net EKE created by baroclinic instability in the WBC is small. Instead, the strong EKE field in the WBC extensions is maintained by barotropic instability near the western boundary and in the near field of the extension (Fig. 5b). Other regions where barotropic instability is important for energizing the eddy field are near the northwest corner of the channel, the tropics, and—to a lesser extent—the subpolar boundary currents. In total, Reynolds stresses account for approximately one-third of the energy put into the eddy field.

Reynolds stresses are usually considered to be a negligible source of eddy kinetic energy because, it is argued, the scales of the mean flow are so much larger than the scales of the eddies as to make direct interaction inefficient (Gill et al. 1974). In the present case, however, the mean circulation contains finescales, particularly in the western boundary currents and their extensions, and the assumption of a spatial spectral gap between the mean and eddy fields does not hold. We

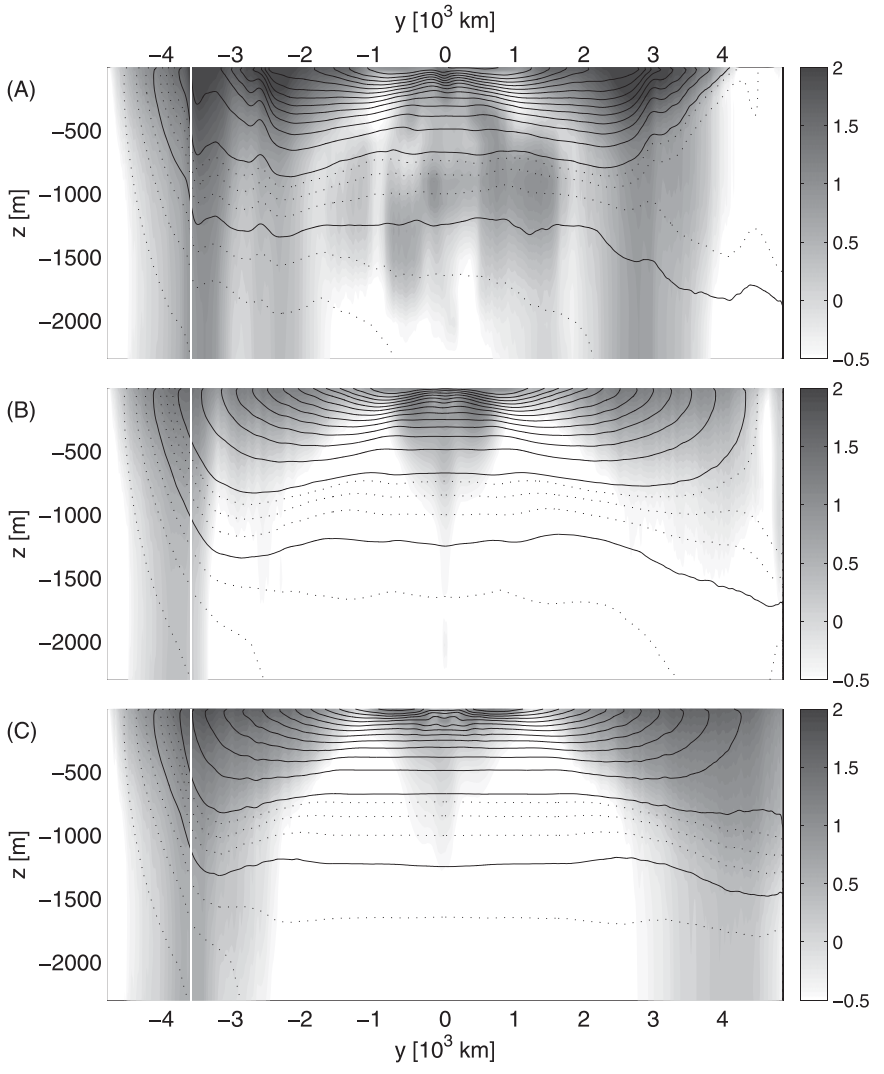

FIG. 4. Temperature (contours) and the $\log_{10}$ of the EKE (shading) in units of J kg^{-1} for the CP case. The contour interval of the solid and dotted lines lines is 1° and 0.25°C, respectively. The northern edge of the channel is shown by a vertical white line. The panel labels correspond to the meridional section labels in Fig. 3.

expect this to be the general case in eddy-resolving ocean simulations.

b. Subpolar and abyssal stratification

The CP configuration corresponds to case 2 outlined in the introduction. If the flow were laminar and the vertical diffusivity sufficiently small, the flow would resemble that illustrated in Fig. 1: the meridional temperature distribution across the surface of the channel south of the outcrop of the deep water would be mapped into a vertical temperature gradient across an abyssal thermocline, which would be sandwiched between nearly isothermal layers of bottom and deep water. In the south, the depth of the abyssal thermocline would be fixed by the depth of the channel topography and the width of the abyssal thermocline set by the diffusivity. The laminar three-layer abyss thus represents a *discontinuous* mapping of the surface temperature gradient across the subpolar gyres into a vertical temperature gradient. In the north, the deep water would split the abyssal thermocline so that its width would no longer be controlled simply by the diffusivity, though its depth would still lie near that of the sill (Vallis 2000).

In the present experiments, the channel topography is missing, but mesoscale eddies allow meridional transport of heat across the channel. The expression of the surface temperature gradient across the channel is no

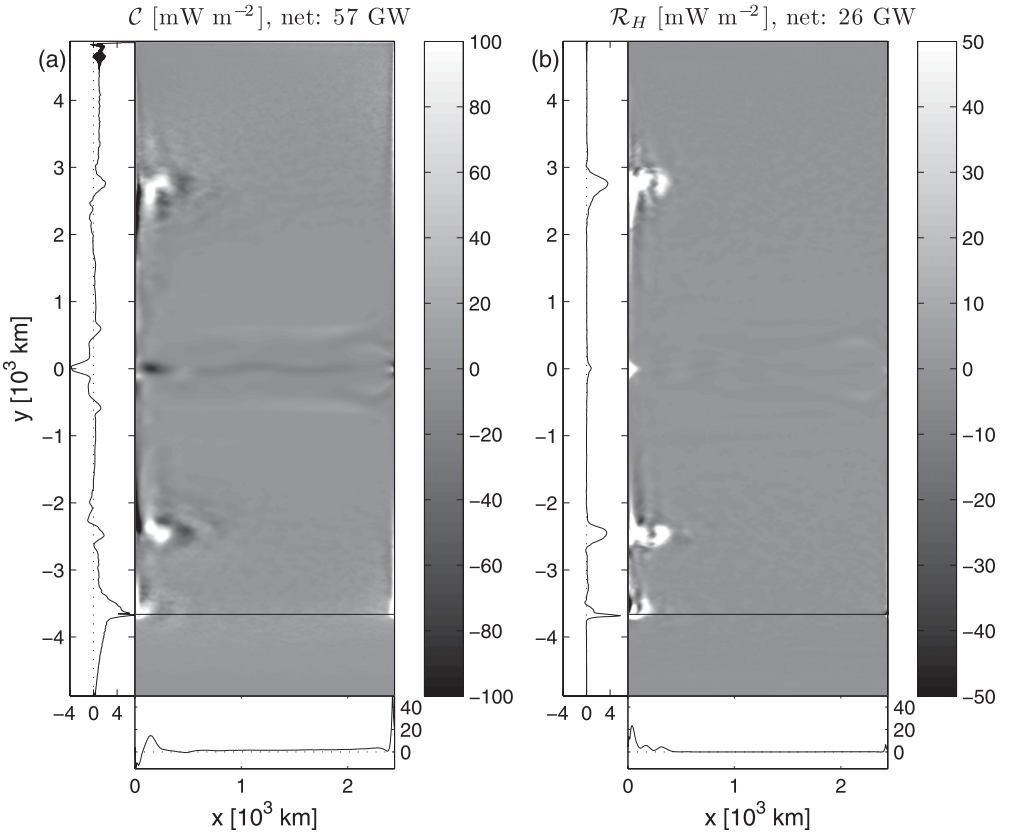

FIG. 5. Vertically integrated rate of energy input into the eddy field due to (a) baroclinic conversion $\mathcal{C}$ and (b) horizontal Reynolds stresses $\mathcal{R}_H$. The plan views have been slightly oversaturated to emphasize detail at low amplitudes and the zonal and meridional integrals of each field are plotted (in units of 10^4 W m^{-1}) to the left and bottom, respectively, of each plan view. The baroclinic conversion rate (a) has been smoothed using a four-point Hann window to remove a grid mode associated with convection.

longer forced into a narrow strip at the level of the topography, and we may expect the abyssal stratification to become a *continuous* mapping of subpolar surface temperatures. The coldest water in the domain is trapped in the channel latitudes (Fig. 4), as with Vallis (2000) in the case with no channel topography; however, most of the surface temperature gradient is expressed as vertical stratification on the northern boundary of the channel. Thus, the abyssal stratification appears to be a *continuous* mapping of the surface gradient across the subpolar gyres.

The deep water (with 1°C $\leq T \leq$ 2°C) appears to spread zonally and meridionally across the entire basin above the bottom water, but is only associated with a distinct thermostad in the northwest corner of the domain (Fig. 4). In the absence of a second tracer (such as salinity), it is impossible to determine the deep-water fraction of the 1°–2°C water away from its source region. A distinct interface between the two water masses is only found in the northern subpolar region where an abyssal thermocline forms at 1600-m depth. Farther south, the abyssal thermocline appears to merge smoothly into the bottom of the main thermocline, and the resulting merged thermocline extends all the way to the bottom.

c. Overturning circulation

The overturning circulation is diagnosed through the time and isopycnally averaged meridional transport of volume:

$$\overline{\psi}(y,\hat{T}) = \overline{\iint\limits_{(x,z):T\leq\hat{T}} v(x,y,z,t)\,dz\,dx} = \psi_{\text{mean}} + \psi_{\text{eddy}}, \quad (4)$$

where

$$\psi_{\text{mean}} = \iint\limits_{(x,z):\overline{T}\leq\hat{T}} \bar{v}\,dz\,dx \quad (5)$$

and $\psi_{\text{eddy}} = \overline{\psi} - \psi_{\text{mean}}$ as defined by Nurser and Lee (2004), where $T = T(x, y, z, t)$; $\overline{(\cdot)}$ is the time average,

and $(\cdot)'$ its deviation. We refer to $\overline{\psi}$ as the "residual overturning streamfunction" in analogy to a similar quantity that appears in transformed Eulerian mean (TEM) theory (see, e.g., Plumb and Ferrari 2005). In practice, $\overline{\psi}$ is computed by using weekly averages of v and T to calculate snapshots of ψ. These snapshots are then averaged to form $\overline{\psi}$. The overturning circulation attributable to the time-mean circulation ψ_{mean} is computed from the time averages of $\overline{v}$ and $\overline{T}$ and then ψ_{eddy}—the correlation between fluctuations in isopycnal height and meridional transport, representing the effect of eddies—is found by difference from $\overline{\psi}$.

A disadvantage of the isopycnally averaged formalism is that height information is lost in the averaging process. Height information may be approximately recovered by remapping $\overline{\psi}$ into nominal height coordinates:

$$\hat{z}(y,\hat{T}) = -H + \frac{1}{L_x}\overline{\iint_{(x,z):T\le\hat{T}} dz\,dx}, \qquad (6)$$

which are easier to interpret visually than temperature coordinates. Equation (6) may be formally inverted to yield $\hat{T}(y,\hat{z})$, which at fixed y gives the temperature $\hat{T}$ of the isotherm that has the zonal and temporal mean height $\hat{z}$.

The residual streamfunction shows the classic three-cell structure of the laminar theory (Fig. 6a, cf. Fig. 1) with a pair of surface cells (difficult to see in Fig. 6a) over a northern-intensified middepth cell and a southern-intensified deep cell. The deep cell originates in the channel latitudes and flows under the middepth cell, penetrating to the northern wall. The middepth cell is somewhat stronger than the deep cell [~7.5 Sv (Sv $\equiv 10^6$ m^3 s^{-1}) compared to ~4 Sv] and occupies the upper 900–1000 m of the water column in the Northern Hemisphere. In the laminar theory the penetration depth of the middepth cell is set by the depth of the sill in the channel and is thus an externally controlled parameter. In the present case, the depth of the middepth cell is determined internally. Approximately half of the middepth transport recirculates within the region of Ekman suction ($y > 2800$ km) while the rest upwells in the subtropics and tropics; about 2 Sv flows across the equator to upwell in the Southern Hemisphere.

The diapycnal flows shown in Fig. 6 are easy to misinterpret as true vertical flows, but there can be a significant discrepancy between the two in the presence of strong zonal isopycnal slopes. For example, the middepth cell appears to downwell through 1000 m near the northern wall as water is transported between the 3° and 1.5°C isotherms, but this flow actually occurs near the surface as the Sverdrup flow returning to the western boundary flows across a zonal surface temperature gradient. This water then subducts to intermediate depths as it flows southward along the western boundary, then flows as part of the Sverdrup flow toward the eastern boundary where it downwells farther. Thus, the zonally integrated picture presented in Fig. 6 masks a complex three-dimensional circulation. Similarly, the apparent sinking along the southern boundary is actually due to water transported horizontally across the surface temperature gradient by the horizontal channel flow; the majority of the actual downwelling occurs near the channel's northern boundary.

While it is straightforward to show that the vertically averaged residual circulation of an ocean subject to steady forcing must be thermally direct (Cessi et al. 2006), in the present case the residual circulation is thermally direct nearly everywhere (with exceptions: e.g., the near-surface residual circulation at $y = 3000$ km is thermally indirect). In contrast, the mean circulation contains regions of vertically averaged thermally indirect flow, most notably in the channel where Ekman divergence brings cold water to the surface where Ekman drift forces it northward against the surface temperature gradient (Fig. 6b). This water then sinks near the northern edge of the channel and is returned southward in the bottom boundary layer. [This is the Deacon cell of Bryan (1991).] The effect of this circulation is to increase the available potential energy of the channel by raising isotherms at the southern edge of the channel and lowering isotherms at the northern edge of the channel. This potential energy is released by mesoscale eddies that drive a circulation in the opposite direction as the mean and is sufficiently strong to overwhelm the signal of the Deacon cell (Fig. 6c).

There are also weak thermally indirect cells in the mean circulation near the surface in the regions of equatorward Ekman transport ($|y| > \pm 2800$ km) outside the channel. The dynamics of these cells is similar to that in the channel except that the vertical extent of the cells is limited by the stronger stratification and the presence of the mean pressure-driven overturning found outside the channel. These thermally indirect cells also tend to increase the local potential energy available to eddies, which in turn drive near-surface, thermally direct cells in both hemispheres (Fig. 6c).

The eddy-induced overturning is generally thermally direct except in the tropics and near the surface in the WBC extensions. In these locations the eddy field is generating available potential energy instead of releasing it, implying a source of eddy energy other than conversion of available potential energy. Indeed, as shown in section 3a(2), most of the net input of EKE in the WBCs and the tropics is due to horizontal shear

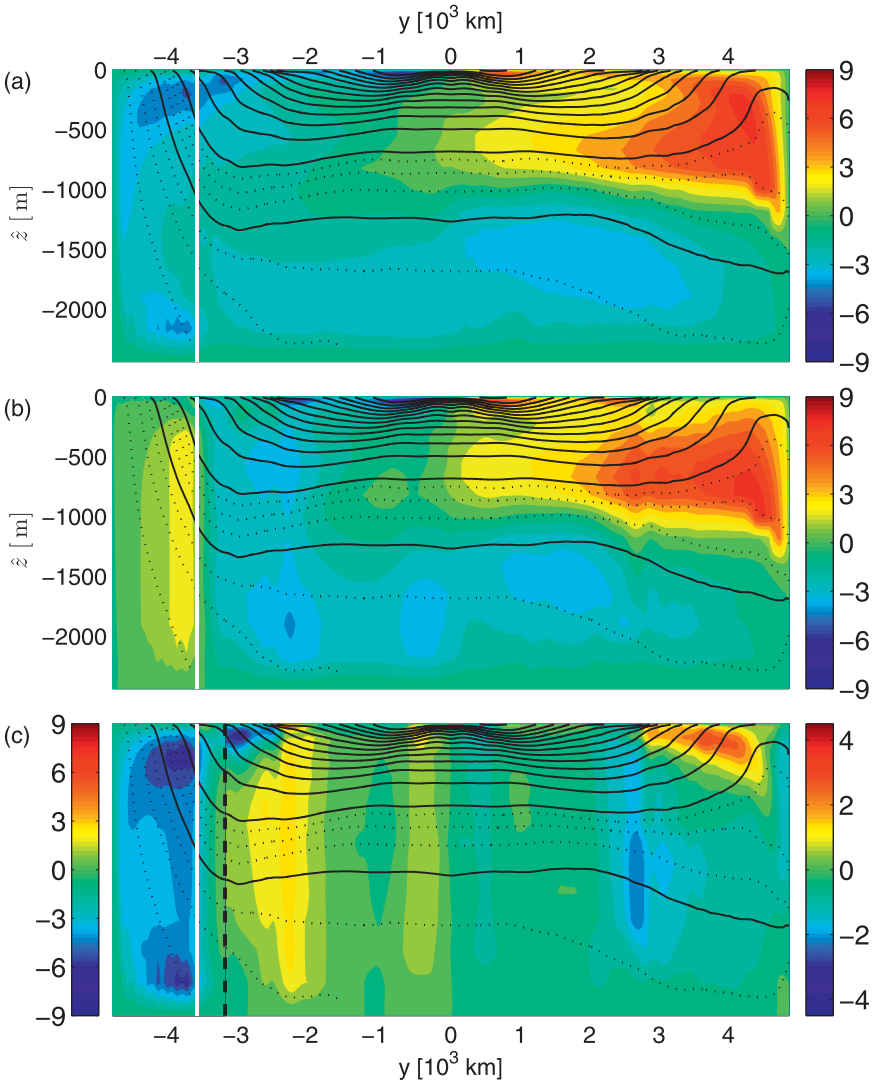

FIG. 6. Isopycnally averaged overturning streamfunction $\overline{\psi}$ (Sv) (colors) for the (a) residual, (b) mean, and (c) eddy flow and temperature field $\hat{T}$ defined in Eq. (6) (contours) for the CP case. The sense of the circulation is clockwise around maxima. The contour interval of the solid and dotted lines is 1° and 0.25°C, respectively. The northern edge of the channel is shown by a vertical white line. The color scale to the right of the vertical dashed line in (c) has been expanded to show greater detail away from the channel.

instabilities. The strength of both the Reynolds and baroclinic conversion terms decay with depth in the WBC extensions, but the decay of the Reynolds conversion is more rapid and the instability mechanism becomes primarily baroclinic below 1000-m depth. In contrast, the equatorial instabilities are shear driven to the ocean bottom. As a consequence, the eddy overturning in the WBC extensions becomes thermally direct at depth but remains thermally indirect throughout the tropics.

Meridional sections of temperature appear to show the deep water as a continuous mass of water stretching from the northern wall to the channel (Fig. 4, also see Fig. 6). It is tempting to interpret this as evidence of a direct advective path between the northern sinking site and the channel. Indeed, some adiabatic theories of the meridional overturning circulation suggest that Northern Hemisphere deep water is upwelled in the channel latitudes, with Ekman suction in the channel providing the "pump" that drives the middepth overturning (Toggweiler and Samuels 1995, 1998). However, the present case is sufficiently diffusive so that the middepth overturning cell upwells in the subtropics and does not extend all the way to the channel (Fig. 6a). Thus, there does not appear to be an advective connection between

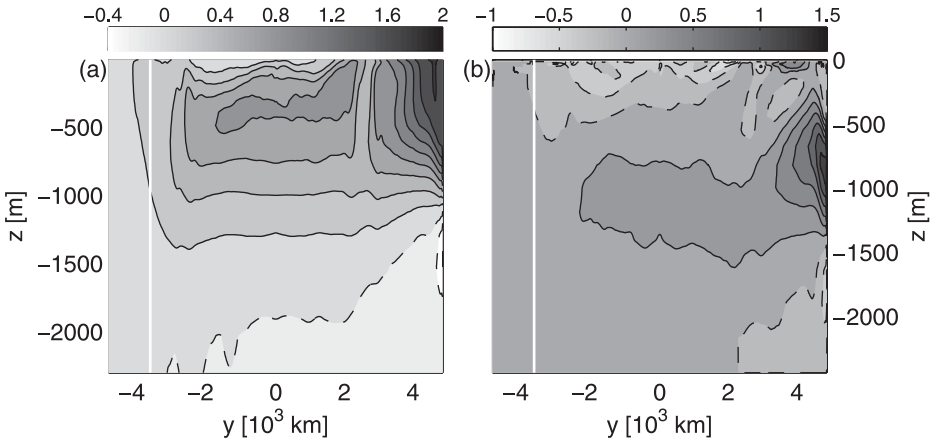

FIG. 7. Difference of the WP zonal mean (a) temperature and (b) buoyancy frequency from the CP case. The contour intervals in (a) and (b) are 0.2°C and 0.2 cph; the zero and negative contours are dashed.

the middepth cell and the channel in the zonal mean. However, the zonal mean may mask a more complex three-dimensional circulation, and an advective connection between the deep water and the channel cannot be ruled out; however, this connection is likely to be weak as it does not appear in the zonal mean.

4. Warm pole experiment

a. Stratification

Warming the north pole by 2.1°C (from 1.2° to 3.3°C) results in a dramatic reduction in the depth and horizontal extent of the northern deep water and a concomitant warming of the upper 1250 m of the water column (Fig. 7a). The most significant warming is found in the northern subpolar gyre, which is directly exposed to the warmer surface temperatures; however, the warming signal penetrates deep into the Southern Hemisphere, with a warming of nearly 1°C in the tropics and southern subpolar gyre and a warming of 0.2°C near the northern edge of the channel.

The removal of the deep-water mass allows the isotherms above and below it to expand into the region that it originally occupied. This allows bottom water to extend farther north, resulting in water near the northern boundary, which is actually colder in the WP case than in the CP case even though the surface temperatures in the former case are everywhere warmer than or equal to the temperatures in the latter case. Additionally, the expansion of these isotherms results in a decrease in the stratification in the upper 500 m as well as in the deepest northern subpolar waters (Fig. 7b). A similar deepening of the main subtropical thermocline was observed by Fučkar and Vallis (2007) in similar numerical experiments using a model with parameterized eddies. In contrast to the laminar theory, the removal of the deep water does not cause the abyss to fill with unstratified bottom or intermediate water (as in the cases with and without the sill described in section 1a). Instead, the abyss remains stratified and the WP case is, in fact, *more* stratified at middepth than the CP case.

b. Overturning circulation

The southern overturning cell dominates the overturning circulation in the WP experiment (Fig. 8a): Its maximum amplitude is nearly 9 Sv, but most of this recirculates in the channel and southern subpolar gyre; only half of the transport penetrates into the southern subtropical gyre and only 3 Sv crosses the equator. The expansion of the southern overturning cell comes at the expense of the northern overturning cell, which is much weaker (~3 Sv) than in the CP case and is confined between the surface and the 3° isotherm at a depth of 500 m. This cell does not cross the equator. As with the CP case, both overturning cells circulate in the thermally direct sense.

The primary difference in the eddy streamfunction of the WP experiment, relative to the CP experiment, is a strengthening of the overturning associated with eddies in the southern WBC extension and a weakening of the corresponding overturning in the northern WBC extension.

Most of the difference between the CP and WP experiments is due to changes in the time-mean circulation, which can, in turn, be explained by changes in the temperature field and simple planetary geostrophic (PG) dynamics. Away from the horizontal boundaries and equator the zonal and vertical PG momentum equations for the perturbation (i.e., WP − CP) meridional velocity v', geopotential ϕ', and temperature T' are

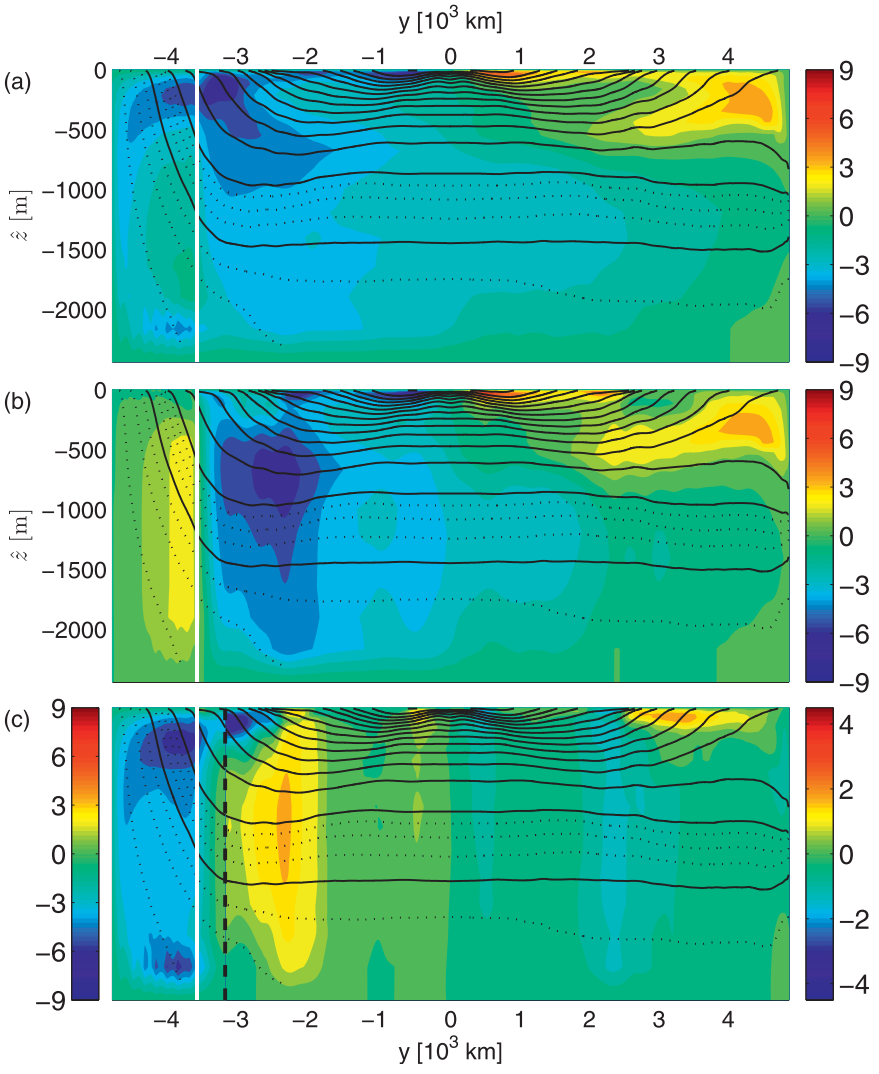

FIG. 8. As in Fig. 6, but for the WP case.

$$f v' = \phi'_x, \tag{7}$$

$$\phi'_z = \alpha g T'. \tag{8}$$

Using the vertical momentum equation to eliminate ϕ' and integrating zonally gives

$$f \int v' dx = \Delta\phi'_B + \alpha g \int_{-H}^{z} \Delta T' dz', \tag{9}$$

where ϕ'_B is geopotential at the bottom and $\Delta(\cdot)$ gives the difference of $(\cdot)$ between the eastern and western boundaries. Here $\Delta\phi'_B$ can be determined by noting that the vertical integral of the lhs must be zeroas there can be no net meridional transport of fluid. Eliminating $\Delta\phi'_B$ gives

$$\int v' dx = \frac{\alpha g}{f}\left[\int_{-H}^{z} \Delta T' dz' - \frac{1}{H}\int_{-H}^{0}\int_{-H}^{z} \Delta T' dz' dz\right] \tag{10}$$

or, equivalently,

$$\psi' = -\frac{\alpha g}{f}\left[\int_{-H}^{z}\int_{-H}^{z'} \Delta T' dz'' dz' - \frac{z+H}{H}\int_{-H}^{0}\int_{-H}^{z} \Delta T' dz' dz\right] \tag{11}$$

when the definition

$$\psi'_z = -\int v' dx \tag{12}$$

is used. The change in the streamfunction estimated from (11) matches that calculated from the model quite well (Fig. 9), indicating that the changes in the overturning streamfunction are largely in thermal wind balance with the changes in the temperature field.

c. Transient adjustment

The adjustment to the WP temperature forcing is very rapid: After only 2 yr, the volume of northern deep water (with $1°C \le T \le 2°C$) is significantly reduced, accompanied by a concomitant increase in the volume of intermediate water (with $3°C \le T \le 5°C$) and, after 13 yr, the water mass adjustment mostly complete (Fig. 10). This adjustment is far too rapid to be explained by a displacement of deep water by southern intermediate water (as argued in Vallis 2000).

Examination of Fig. 10 shows that the most likely source of water to displace the northern deep water is northern intermediate water formed near the boundary between the northern subtropical and subpolar gyres; this water is visible near $y = 3000$ km in the CP run (Fig. 10a, thick solid line). The initial volume of this water, combined with additional water in the same temperature range formed by the WP temperature forcing, is more than adequate to explain the increase in intermediate water and decrease in deep water seen in Fig. 10. This local response then propagates throughout the rest of the basin via a series of coastal and equatorial Kelvin waves (not shown), much like those described by Kawase (1987). By the end of the adjustment the volume of southern deep water is essentially unchanged in the WP case and the southern intermediate water layer is only slightly thicker, consistent with the general warming of the middepth waters. The fact that this thickening propagates from north to south again argues for a northern source of the additional intermediate water.

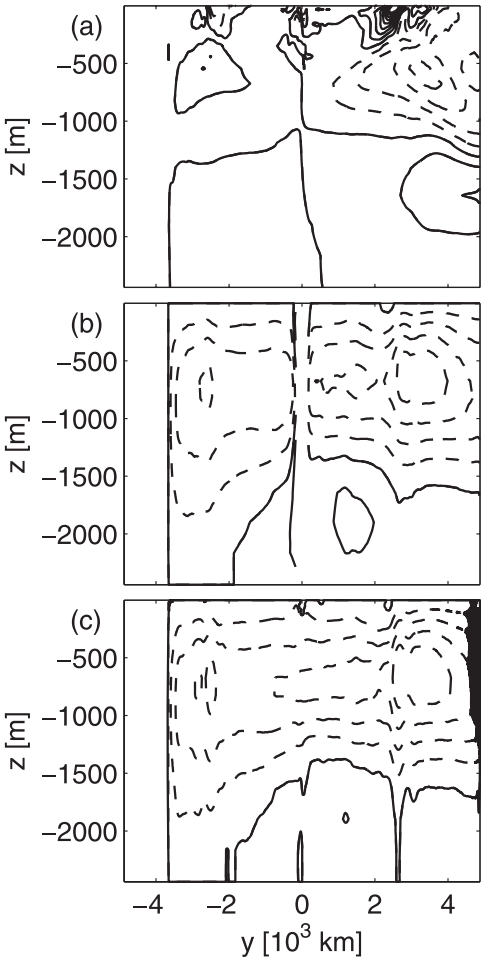

FIG. 9. (a) Change $\Delta T'$ in the east − west temperature difference between the CP and WP experiments, (b) change in the mean overturning streamfunction ψ' estimated from Eq. (11), and (c) change in the mean overturning streamfunction ψ' calculated from the model. The contour interval is (a) 0.25°C and (b), (c) 1 Sv; negative contours are dashed. (b) The equator has been masked out.

d. Mechanism

If deep-water formation is not shut down by an invasion of southern intermediate water, what explains the dramatic difference between the CP and WP cases? A possible mechanism is the following: The isothermal slope in the channel is set by a competition between the wind forcing, which tries to overturn the isotherms, and the eddies, which try to flatten the isotherms. A complete theory should predict the isothermal slopes in the channel; here, we will take them as given. since the wind and thermal forcing over the channel are the same in both CP and WP cases, the isothermal slopes in the channel are nearly the same. As a first approximation, suppose that the depth of the isotherms in the enclosed part of the basin is fixed by the depth that they achieve on the northern edge of the channel, except where they must outcrop (to prevent static instabilities) and where they encounter the wind-driven subtropical circulation (which deforms them downward).

In the CP case, the deep water (with $1°C \le T \le 2°C$) is exposed to the surface in the northern subpolar region. This means that the 2° and 3°C isotherms must outcrop before reaching the northern wall. This forces them up toward the base of the main thermocline, which increases the stratification there and, in turn, leads to stronger diathermal upwelling through the base of the main thermocline (Fig. 11a). The primary source for this upwelling is the water below the 2°C isotherm—that is, the deep water. Thus, the fact that the 2° and 3°C outcrop leads to a strong middepth overturning cell.

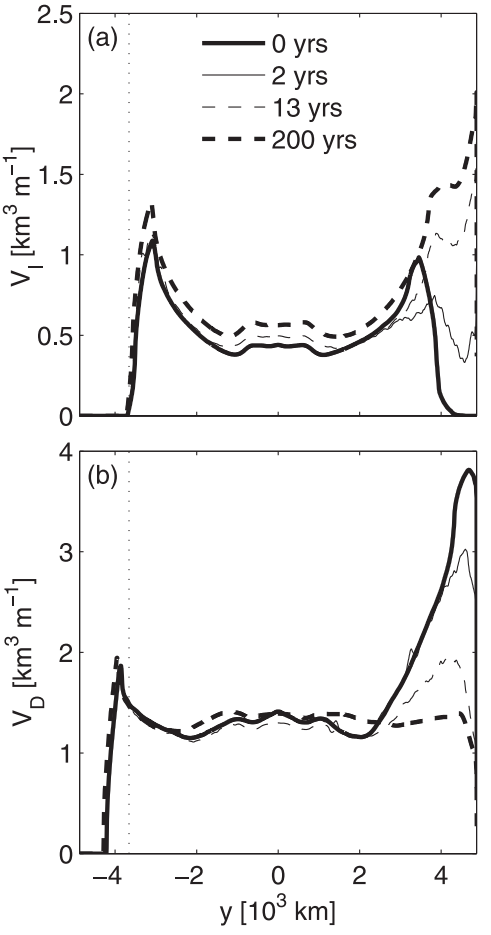

FIG. 10. Volume of (a) intermediate (V_I) and (b) deep (V_D) water in the CP case (thick, solid) and 2 (thin, solid), 13 (thin, dashed), and 200 (thick, dashed) years after the transition to WP temperature forcing.

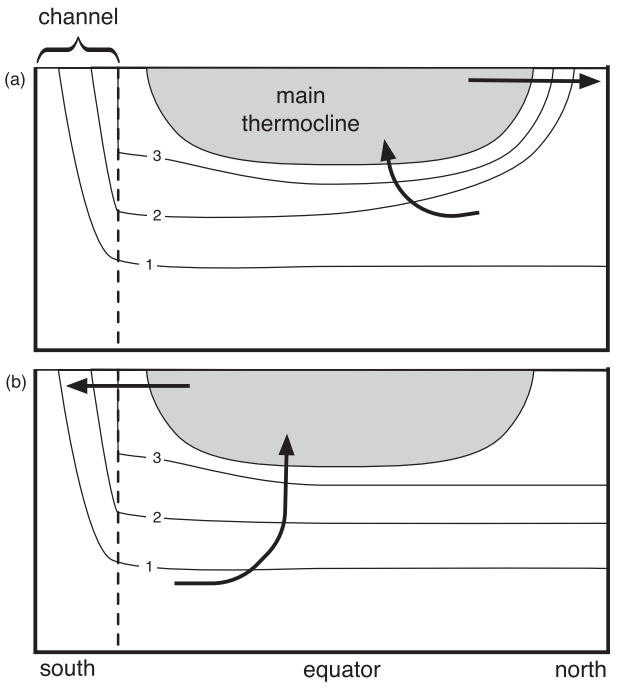

FIG. 11. Mechanism for the different circulation patterns in the (a) CP and (b) WP cases. See the text for explanation.

In the WP case, neither the 2° nor the 3°C isotherm must outcrop, so both maintain the depth set when they exited the channel, except where deformed downward by the wind-driven circulation (Fig. 11b). Thus, the stratification at the base of the main thermocline is weaker—especially in the north—and there is a commensurate decrease in the deep-water upwelling rate and the strength of the deep cell. However, while the stratification at the base of the main thermocline is reduced, the stratification at middepth is increased. This increases the upwelling through 1° and 2°C isotherms, but now the only source of water for this upwelling is the south, which increases the strength of the deep cell.

Note that, in the above mechanism, the primary role of the channel is to set the scale depth for the abyssal stratification; the mechanism itself does not require the channel to explain the weakening of the deep cell. The argument could be repeated without the channel with the same result, except that the abyssal isotherms would be higher in the water column and the abyssal stratification would be weaker, as isotherms tend to be shallower outside of the channel. This argues that the condition put forth by Vallis (2000)—that the deep water must have a density in the range of those found in the channel for a strong middepth cell—no longer holds when the effect of eddies is taken into account. Indeed, in a series of experiments in which eddies were parameterized, Fučkar and Vallis (2007) found that that the middepth cell weakened as the northern temperature increased relative to the southern temperature but that there was no catastrophic collapse of the middepth cell as the northern temperature exceeded the range of those found in the channel.

5. Heat flux

a. Meridional heat flux

In the CP experiment, 16 TW of heat is transported northward across the equator, driven by the strong middepth overturning circulation. At slightly more than 10% of the maximum poleward heat flux at midlattitudes, this value of interhemispheric heat transport is consistent with that found in more realistic models (e.g., Maltrud and McClean 2005) when the small width and depth of the present model are accounted for. The eddy heat transport acts to oppose the mean transport and is thus equatorward in the vicinity of the WBC

extensions and in the tropics. The equator is cooled due to equatorial upwelling, so the equatorward eddy heat flux in the tropics is down the zonally averaged meridional temperature gradient. In contrast, the eddy heat transport in WBC extensions is up the zonally averaged meridional temperature gradient, but down the local temperature gradient since the WBC extensions are warmer than the open ocean water equatorward of them. Such eddy heat fluxes counter to the large-scale temperature gradient have also been observed in the Gulf Stream (Wunsch 1999).

The Northern Hemisphere is significantly warmer than the Southern Hemisphere in the WP experiment and exports a large amount of heat (68 TW) into the Southern Hemisphere. As the middepth circulation does not cross the equator, this heat flux is the result of cold bottom water that crosses the equator at great depth, is warmed by downward heat flux in the Northern Hemisphere, and returns to the Southern Hemisphere at middepth. Again, the effect of the eddies is to oppose the poleward mean heat flux in the tropics and WBC extensions and the equatorward mean heat flux in the channel.

As with the overturning circulation, most of the difference between the two cases is captured by changes in the mean heat flux (Fig. 12). The eddy heat fluxes in the subtropics are largely controlled by the baroclinicity of the western boundary currents, which is determined primarily by the wind over the subtropical gyres, while the eddy heat flux in the tropics is controlled by the local surface forcing. Since neither wind nor tropical surface forcing is changed between the two cases, the tropical and subtropical eddy heat fluxes are nearly identical in the two cases aside from a slight shift in the location of the northern extremume of the eddy heat transport associated with a similar shift in the location of the WBC extension.

The eddy heat fluxes in the subpolar regions respond more strongly to the change in thermal forcing. The warming reduces the surface temperature gradient across the northern subpolar gyre, which reduces the potential energy available to form eddies and the northern subpolar eddy heat flux is reduced in the WP case. Conversely, the temperature gradient across, and thus the available potential energy in, the channel is increased by the warming of the upper 1000 m of the water column, observed in the previous section (Fig. 7a), and the eddy heat flux across the channel is increased in the WP case.

b. Vertical heat flux

The role of different physical processes in the vertical heat flux can be assessed on a basin-by-basin basis by examining the horizontally integrated heat equation

$$\langle \bar{w}\bar{\mathcal{H}}\rangle_z + \int \bar{v}\bar{\mathcal{H}}\Big|_{y_1}^{y_2} dx + \langle \overline{w'\mathcal{H}'}\rangle_z + \int \overline{v'\mathcal{H}'}\Big|_{y_1}^{y_2} dx = \kappa\langle \bar{\mathcal{H}}\rangle_{zz}, \tag{13}$$

where $\mathrm{H} = \rho c_p T$ is the specific heat content of the fluid and angle brackets represent the horizontal integral over the area defined by $0 \le x \le L_x$, $y_1 \le y \le y_2$. The horizontal diffusion term can be verified to be utterly negligible and the surface diabatic forcing term is excluded by focusing attention below the surface layer. Following Paparella and Young (2002), we vertically integrate Eq. (13) from $-H$ to z and make use of the bottom boundary condition $w = \mathcal{H}_z = 0$, giving

$$\underbrace{\langle \bar{w}\bar{\mathcal{H}}\rangle + \int_{-H}^{z}\int \bar{v}\bar{\mathcal{H}}\Big|_{y_1}^{y_2} dx\, dz'}_{\mathcal{M}} + \underbrace{\langle \overline{w'\mathcal{H}'}\rangle + \int_{-H}^{z}\int \overline{v'\mathcal{H}'}\Big|_{y_1}^{y_2} dx\, dz'}_{\mathcal{E}} \underbrace{-\kappa\langle \bar{\mathcal{H}}\rangle_z}_{\mathcal{D}} = 0 : \tag{14}$$

$\mathcal{M}$ and $\mathcal{E}$ represent the vertical heat flux due to mean and eddy advection, respectively, and $\mathcal{D}$ represents the vertical heat flux due to diffusion.[1] Equation 14 is a generalization of the quasi-vertical heat budget considered by Munk and Wunsch (1998). There is not a separate term describing the vertical heat flux due to convection since the convective flux is a component of the eddy advective flux. There appears to be no practical way to separate the two components. Indeed, this separation may not even be meaningful in general because upright convection quickly gives way to slantwise convection (i.e., baroclinic instability) in the presence of lateral buoyancy gradients (Marshall et al. 1998). Experiments where upright convection was parameterized by an enhanced vertical diffusivity show that upright convection contributes significantly to the heat budget only in the upper 200 m of the water column and that the sum of the eddy and convective heat flux in those

[1] As pointed out by a reviewer, $\mathcal{M}$ and $\mathcal{E}$ only represent true vertical heat fluxes when the average is taken over the entire domain. For regions smaller than the domain size, the horizontal convergence of heat into the box below the level z must be subtracted from the vertical flux of heat through z to remove the (physically insignificant) rotational component of the flux. The combined quantity is an integrated heat flux divergence. In either case, the interpretation of the flux (divergence) is the same: downward (negative) and upward (positive) values of the flux (divergence) tend to cool and warm, respectively, the box below the level z.

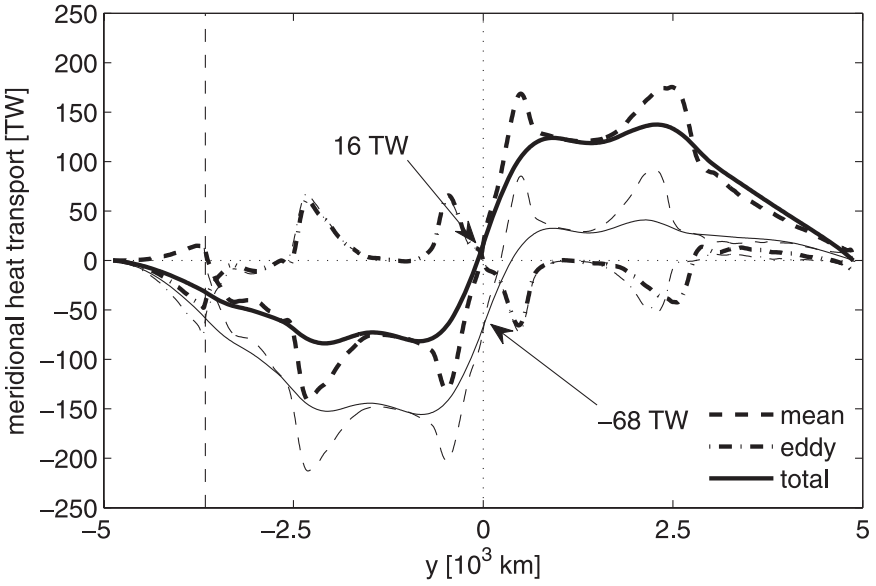

FIG. 12. Meridional heat transport. The thick and thin curves show the CP and WP values, respectively. The cross-equatorial heat transport is indicated by arrows.

experiments is nearly identical to the eddy heat flux in the present model.

In the global integral, both diffusion and the mean flow act to transport heat downward, which acts to destratify the water column (Fig. 13a). The ocean is restratified by the eddy flow, which transports heat upward. Since the mean heat flux is downward at nearly every level, the mean flow is a source of available potential energy; that is, the mean flow is thermally indirect.

For the surface temperature field in the present study, the thermal sense of the mean flow is determined partially by the sign of the Ekman pumping: Ekman pumping tends to drive thermally direct flow, while Ekman suction tends to drive thermally indirect flow (Cessi et al. 2006). Accordingly, we examine the vertical heat budget in three regions, determined by the sign of the Ekman pumping: the southern subpolar (SSP) region (Ekman suction), the subtropics (Ekman pumping; the tropics are also included for simplicity), and the northern subpolar (NSP) region (Ekman suction). As expected, the mean flow is thermally indirect in the SSP region (Fig. 13b) and near the surface in the NSP region (Fig. 13d) and thermally direct in the subtropics (Fig. 13c). The mean advective heat flux divergence in the subpolar regions is sufficiently negative to completely overwhelm the positive mean advective heat flux divergence in the subtropics so that the globally integrated mean advective heat flux is downward.

The eddy heat flux divergence in the SSP region largely cancels the mean advective heat flux divergence, leaving diffusion as a small residual (Fig. 13b). The NSP region shows a balance similar to the SSP region in the upper 500 m, though diffusion plays a larger role (Fig. 13d).

The mean advective heat flux divergence is positive at all depths in the subtropics and is primarily opposed by diffusion except near the surface where eddy fluxes are important (Fig. 13c). The eddy heat flux divergence is positive (augmenting the mean advective heat flux divergence) near the surface but negative in the depth ranges 160–750 m and 1800 m to the bottom. For these depth ranges the eddies are thus a *source* of available potential energy in the subtropics rather than a sink. While the current decomposition does not allow us to exclude the possibility that the eddies are simply fluxing available potential energy into the subtropics through the side boundaries, the presence of strong, thermally indirect circulations in the eddy overturning streamfunction associated with shear and inertial instabilities (Figs. 5b and 6c) implies that the source of the available potential energy is within the subtropics.

The fact that the global mean advective and diffusive heat fluxes are in the same direction has significant consequences: First, it implies that the eddies are qualitatively important in determining the global mean flow because the heat budget could not be closed if the eddies were removed without either a qualitative change in the mean circulation or an additional physical process to transport heat vertically. Second, the advective–diffusive balance

$$\mathcal{M} + \mathcal{D} \approx 0 \tag{15}$$

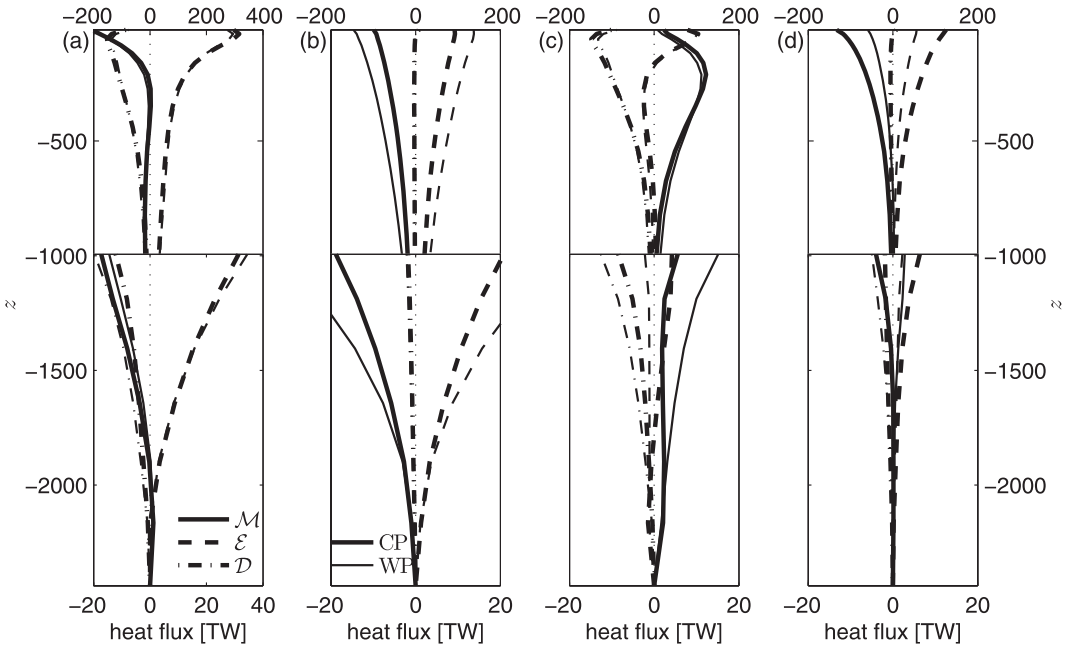

FIG. 13. Components of heat flux divergence as defined in Eq. (14) averaged over (a), (e) the whole domain; (b), (f) the southern subpolar gyre (defined as the southern region Ekman suction); (c), (g) the subtropics and tropics; and (d), (h) the northern subpolar gyre for the (top) CP case and (bottom) difference between the WP and CP cases. The abscissa has been contracted below 800 m to show detail in the abyss.

advanced by Munk (1966) and Munk and Wunsch (1998) cannot hold globally, as both terms in (15) have the same sign. In the subtropics, however, the mean and diffusive fluxes are in opposite directions, and we might recover the Munk and Wunsch (1998) balance [indeed, Munk and Wunsch (1998) is formulated in the subtropics]. The implied average vertical diffusivity would, however, be over- or underestimated depending the extent that $\mathcal{E}$ cancels or augments, respectively, the sum $\mathcal{M} + \varepsilon$.

The response to the Northern Hemisphere warming in the WP case is concentrated in the subpolar regions, where both the mean advective and eddy heat flux divergence decrease in the Northern Hemisphere (Fig. 13h) and increase in the Southern Hemisphere by roughly a factor of 2 (Fig. 13f). In the NSP region, this can be explained by a decrease in baroclinicity due to the decreased surface temperature gradient, which reduces the strength of the mean middepth cell and the pool of potential energy available to drive the eddies. The opposite effect occurs in the SSP region, where the warming in the upper 1000 m of the subtropics increases the baroclinicity of the SSP region. In the upper few hundred meters, some of the change in the subpolar eddy heat flux may be due to decreased convection in the north (due to warmer surface forcing) and increased convection in the south (due to warmer water temperatures).

As discussed in section 4, the WP case has a less stratified main thermocline and more stratified middepth in the subtropics than the CP case. This change in stratification is reflected in the change in the subtropical diffusive flux (Fig. 13g), which is weaker at thermocline depths and stronger at middepth, consistent with the mechanism discussed in section 4d. The eddy flux divergence is thus even more strongly thermally indirect in the WP case than in the CP. The augmentation of the mean advective flux below 300 m is consistent with the increased strength of the upwelling limb of the deep cell in the subtropics.

Since the diffusive flux divergence in each of the subpolar regions is relatively unchanged, the change in the global diffusive flux is due entirely to the change in the subtropics. The global advective fluxes are primarily determined by the residual between the two subpolar regions and show decreased eddy fluxes above 400 m and increased eddy fluxes below. The mean advective fluxes follow an opposite pattern.

6. Conclusions

Though the eddy-resolving simulations of the large-scale meridional overturning circulation presented here are consistent with some of the important predictions of the laminar theory, there are important and interesting differences.

Specifically, we find that, if the north pole temperature is sufficiently warm, the formation of northern deep water is suppressed and the middepth cell is small and weak while the deep cell is large and vigorous. In contrast, if the north pole temperature is in the range of the southern channel temperatures, the middepth cell is large and strong, while the deep cell has a reduced amplitude. While this appears to verify a critical prediction of the laminar theory, the manner in which these changes occur is quite different. In the laminar theory, the formation of northern deep water is suppressed by an invasion of southern intermediate water, while in the present case the intermediate water appears to come from the Northern Hemisphere. A simple mechanism explaining the differences between the two experiments is outlined. Interestingly, while the channel sets the scale depth for the abyssal stratification, the mechanism does not appear to require that the northern temperature to have a special relationship to the channel temperatures; it is merely sufficient that the northern temperatures are cold enough. It will require more experiments at intermediate values of the pole-to-pole temperature difference to confirm this finding in the present model, though we note that Fučkar and Vallis (2007) found a similar result in a model wherein the effects of eddies were parameterized.

In the laminar theory, the formation of realistic deep stratification depends on both the existence of a sill in the channel and the ability of the northern deep water to split the abyssal thermocline, which broadens what would be a very narrow vertical region of stratification. In the present case, there is no channel topography and the abyss is well stratified even in the warm pole case. In fact, having the north pole temperature in the range of the southern channel temperatures leads to *weaker* deep stratification.

Eddies were found to be qualitatively important in maintaining the circulation in both the CP and WP cases because they allow cross-channel heat transport and balance the globally thermally indirect mean circulation. However, most of the difference between the overturning circulations in the CP and WP cases could be explained by changes in the mean overturning circulation, which is largely in thermal wind balance with changes in the temperature field.

Examination of the eddy kinetic energy budget finds that Reynolds stresses are responsible for almost one-third of the energy input into the eddy field. This is a significant result because the direct coupling between the mean and eddy flows is normally considered negligible.

In most regions, meridional and vertical eddy heat fluxes oppose the mean heat flux. In the subpolar regions, the vertical mean and eddy fluxes cancel to such an extent that the diffusion is a small residual. Additionally, in these regions and in the global average, the mean and diffusive heat fluxes are in the same direction, implying that eddies are qualitatively important in the vertical heat budget. This makes a Munk (1966)-type advective–diffusive balance impossible.

That the mean and diffusive heat fluxes should be in the same direction is a consequence of the energetics of baroclinic eddies: A net conversion of potential energy, $\mathcal{C}$, into EKE implies that the globally integrated eddy heat flux is upward, as $\mathcal{C}$ is proportional to $\overline{w'\mathcal{H}'}$ by (1). If the globally integrated mean heat flux were also upward, the combined mean and eddy advective heat fluxes would require a large downward diffusive heat flux and thus a substantially diabatic ocean. With a downward globally integrated mean heat flux (i.e., in the same direction as diffusion), the mean and eddy heat fluxes partially cancel and the required diffusive flux is reduced. Because the World Ocean is observed to be full of baroclinic eddies (Wunsch 1998) and largely adiabatic below the mixed layer (Gregg 1989), the latter case is appropriate for the modern ocean. One way to force our model ocean into the highly diabatic state is to unrealistically reverse the surface wind with the same buoyancy forcing (experiment not shown). The reversed wind then drives a thermally direct mean circulation that advects heat in the same direction as the eddies and the diffusive flux must nearly double to close the vertical heat budget. It would be interesting to determine whether the World Ocean was ever in a highly diabatic state in the past and what the resulting consequences for world climate were.

Much work remains to be done. The response of the system to systematic variations in the external parameters needs to be assessed. Most importantly, the diffusivity in the present case is rather large $\kappa \approx 10^{-4}$ $m^2\ s^{-1}$ and the effects of lower diffusivities need to be determined. This is a subject of ongoing research.

Acknowledgments. The authors acknowledge the support of the DOE under the SciDAC program. Computational resources were provided by the San Diego Supercomputer Center, the National Center for Computational Sciences, and the National Energy Research Scientific Computing Center. We thank Bill Young for helpful discussions and suggestions. The suggestions of two anonymous reviewers significantly improved this text.

REFERENCES

Bryan, K., 1991: Ocean circulation models. *Strategies for Future Climate Research,* M. Latif, Ed., Max-Planck Institut für Meteorologie, 265–286.

Cessi, P., and M. Fantini, 2004: The eddy-driven thermocline. *J. Phys. Oceanogr.,* **34,** 2642–2658.

——, W. R. Young, and J. A. Polton, 2006: Control of large-scale heat transport by small-scale mixing. *J. Phys. Oceanogr.,* **36,** 1877–1894.

Fučkar, N. S., and G. K. Vallis, 2007: Interhemispheric influence of surface buoyancy conditions on a circumpolar current. *Geophys. Res. Lett.,* **34,** L14605, doi:10.1029/2007GL030379.

Gill, A. E., J. S. A. Green, and A. J. Simmons, 1974: Energy partition in the large-scale ocean circulation and the production of mid-ocean eddies. *Deep-Sea Res.,* **21,** 499–529.

Gregg, M. C., 1989: Scaling turbulent dissipation in the thermocline. *J. Geophys. Res.,* **94,** 9686–9698.

Griesel, A., and M. A. M. Maqueda, 2006: The relation of meridional pressure gradients to North Atlantic Deep Water volume transport in an ocean general circulation model. *Climate Dyn.,* **26,** 781–799.

Hallberg, R., and A. Gnanadesikan, 2006: The role of eddies in determining the structure and response of the wind-driven Southern Hemisphere overturning: Results from the Modeling Eddies in the Southern Ocean (MESO) project. *J. Phys. Oceanogr.,* **36,** 2232–2252.

Hellerman, S., and M. Rosenstein, 1983: Normal monthly wind stress over the world ocean with error estimates. *J. Phys. Oceanogr.,* **13,** 1093–1104.

Henning, C. C., and G. K. Vallis, 2004: The effects of mesoscale eddies on the main subtropical thermocline. *J. Phys. Oceanogr.,* **34,** 2428–2443.

——, and ——, 2005: The effects of mesoscale eddies on the stratification and transport of an ocean with a circumpolar channel. *J. Phys. Oceanogr.,* **35,** 880–896.

Hill, C., A. Adcroft, D. Jamous, and J. Marshall, 1999: A strategy for terascale climate modeling. *Proc. Eighth ECMWF Workshop on the Use of Parallel Processors in Meteorology,* Reading, United Kingdom, ECMWF, 406–425.

Kamenkovich, I. V., and E. S. Sarachick, 2004: Mechanisms controlling the sensitivity of the Atlantic thermohaline circulation to the parameterization of eddy transports in ocean GCMs. *J. Phys. Oceanogr.,* **34,** 1628–1647.

Karsten, R. H., H. Jones, and J. Marshall, 2002: The role of eddy transfer in setting the stratification and transport of a circumpolar current. *J. Phys. Oceanogr.,* **32,** 39–54.

Kawase, M., 1987: Establishment of deep ocean circulation driven by deep-water production. *J. Phys. Oceanogr.,* **17,** 2294–2317.

Maltrud, M. E., and J. L. McClean, 2005: An eddy resolving global 1/10° ocean model. *Ocean Modell.,* **8,** 31–54.

Marshall, J., and T. Radko, 2006: A model of the upper branch of the meridional overturning of the Southern Ocean. *Prog. Oceanogr.,* **70,** 331–345.

——, H. Jones, and C. Hill, 1998: Efficient ocean modeling using non-hydrostatic algorithms. *J. Mar. Syst.,* **18,** 115–134.

——, ——, R. Karsten, and R. Wardle, 2002: Can eddies set ocean stratification? *J. Phys. Oceanogr.,* **32,** 26–38.

Munk, W. H., 1966: Abyssal recipes. *Deep-Sea Res.,* **13,** 707–730.

——, and C. Wunsch, 1998: Abyssal recipes II: Energetics of tidal and wind mixing. *Deep-Sea Res. I.,* **45,** 1977–2010.

Nurser, A. J. G., and M.-M. Lee, 2004: Isopycnal averaging at constant height. Part I: The formulation and a case study. *J. Phys. Oceanogr.,* **34,** 2721–2739.

Paparella, F., and W. R. Young, 2002: Horizontal convection is non-turbulent. *J. Fluid Mech.,* **466,** 205–214.

Pedlosky, J., 1987: *Geophysical Fluid Dynamics*. 2nd ed. Springer-Verlag, 710 pp.

——, 2003: Thermally driven circulations in small oceanic basins. *J. Phys. Oceanogr.,* **33,** 2333–2340.

——, and M. Spall, 2005: Boundary intensification of vertical velocity in a β-plane basin. *J. Phys. Oceanogr.,* **35,** 2487–2500.

Plumb, R. A., and R. Ferrari, 2005: Transformed Eulerian-mean theory. Part I: Nonquasigeostrophic theory for eddies on a zonal-mean flow. *J. Phys. Oceanogr.,* **35,** 165–174.

Radko, T., 2005: Analytical solutions for the ACC and its overturning circulation. *J. Mar. Res.,* **63,** 1041–1055.

——, and J. Marshall, 2004: Eddy-induced diapycnal fluxes and their role in the maintenance of the thermocline. *J. Phys. Oceanogr.,* **34,** 372–383.

Salmon, R., 1990: The thermocline as an ''internal boundary layer.'' *J. Mar. Res.,* **48,** 437–469.

Samelson, R. M., 1999: Geostrophic circulation in a rectangular basin with a circumpolar connection. *J. Phys. Oceanogr.,* **29,** 3175–3184.

——, 2004: Simple mechanistic models of middepth meridional overturning. *J. Phys. Oceanogr.,* **34,** 2096–2103.

——, and G. K. Vallis, 1997: Large-scale circulation with small diapycnal diffusion: The two-thermocline limit. *J. Mar. Res.,* **55,** 223–275.

Spall, M., 2003: On the thermohaline circulation in semi-enclosed marginal seas. *J. Mar. Res.,* **61,** 1–25.

Stommel, H., and J. Webster, 1962: Some properties of the thermocline equations in a subtropical gyre. *J. Mar. Res.,* **44,** 695–711.

Toggweiler, J. R., and B. Samuels, 1995: Effect of Drake Passage on the global thermohaline circulation. *Deep-Sea Res. I.,* **42,** 477–500.

——, and ——, 1998: On the ocean's large-scale circulation near the limit of no vertical mixing. *J. Phys. Oceanogr.,* **28,** 1832–1852.

Vallis, G. K., 2000: Large-scale circulation and production of stratification: Effects of wind, geometry, and diffusion. *J. Phys. Oceanogr.,* **30,** 933–954.

——, 2006: *Atmospheric and Oceanic Fluid Dynamics: Fundamentals and Large-Scale Circulation*. Cambridge University Press, 745 pp.

Veronis, G., 1975: The role of models in tracer studies. *Numerical Models of the Ocean Circulation*, National Academy of Sciences, 133–146.

Wunsch, C., 1998: The work done by the wind on the oceanic general circulation. *J. Phys. Oceanogr.,* **28,** 2332–2340.

——, 1999: Where do ocean eddy heat fluxes matter? *J. Geophys. Res.,* **104,** 13 235–13 249.

Young, W. R., and G. R. Ierley, 1986: Eastern boundary conditions and weak solutions of the ideal thermcline equations. *J. Phys. Oceanogr.,* **16,** 1884–1900.